

# Layer-skipping connections improve the effectiveness of equilibrium propagation on layered networks

Jimmy Gammell<sup>1,\*</sup>, Sonia M. Buckley<sup>1</sup>, Sae Woo Nam<sup>1</sup> and Adam N. McCaughan<sup>1</sup>

<sup>1</sup>*National Institute of Standards and Technology, Boulder, CO, United States*

Correspondence\*:

Jimmy Gammell

jimmy.gammell@colorado.edu

## 2 ABSTRACT

3 Equilibrium propagation is a learning framework that marks a step forward in the search for a  
4 biologically-plausible implementation of deep learning, and could be implemented efficiently in  
5 neuromorphic hardware. Previous applications of this framework to layered networks encountered  
6 a vanishing gradient problem that has not yet been solved in a simple, biologically-plausible way.  
7 In this paper, we demonstrate that the vanishing gradient problem can be overcome by replacing  
8 some of a layered network's connections with random layer-skipping connections. We additionally  
9 compare the computational complexities of equilibrium propagation and backpropagation to show  
10 that it would be easier to implement the former in neuromorphic hardware.

11 **Keywords:** equilibrium propagation, deep learning, small-world, layer-skipping connections, neuromorphic computing, biologically-  
12 motivated

13 **Number of words:** 3152

14 **Number of figures:** 7

15 **Number of tables:** 1

## 1 INTRODUCTION

16 As research into neural networks grows, there has been increased interest in designing biologically-inspired  
17 training algorithms, as they may offer insight into biological learning processes and also offer clues  
18 towards developing energy-efficient neuromorphic systems [Wozniak et al., 2018; Crafton et al., 2019;  
19 Ernout et al., 2020; Bartunov et al., 2018; Lillicrap et al., 2014; Bengio et al., 2015]. The equilibrium  
20 propagation learning framework developed Scellier and Bengio [2016] is one such algorithm. It is a  
21 method for training a class of energy-based networks, the prototype for which is the continuous Hopfield  
22 network Hopfield [1984]. In particular, it addresses one of the major issues that prevent other training  
23 algorithms (such as backpropagation) from being biologically-plausible, which is the requirement for  
24 separate computation pathways for different phases of training. This also makes the algorithm appealing for

practical implementation into neuromorphic hardware, because only a single computation circuit is required within each (non-output) neuron, rather than multiple distinct circuits. However, current implementations of the algorithm still have a defect that diminishes its biological plausibility: they require hand-tuned per-layer hyperparameters to account for a vanishing gradient through the network. In addition to not being biologically plausible, these multiplicative hyperparameters would be difficult to implement in a neuromorphic hardware system with limited bit depth. In this work, we demonstrate that the vanishing gradient problem can instead be addressed through topological means: by randomly replacing some of a layered network’s connections with layer-skipping connections, we can generate a network that trains each layer more evenly and does not need per-layer hyperparameters.

Implementation of equilibrium propagation in [Scellier and Bengio, 2016] was hindered by a vanishing gradient problem whereby networks with as few as 3 hidden layers trained slowly on MNIST [LeCun and Cortes, 1998] – a serious issue given that network depth is critical to performance on difficult datasets [Simonyan and Zisserman, 2014; Srivastava et al., 2015b] and that convergence to a low error rate on MNIST is a low bar to meet. The problem was overcome in [Scellier and Bengio, 2016] by independently tuning a unique learning rate for each layer in the network. These learning rates were multiplicative factors that proportionally scaled the signals communicated between layers.

In our work, we have modified the strictly-layered topology of the original implementation by adding and removing connections to create a small-world-like network [Watts and Strogatz, 1998]. Through this modification we have eliminated the per-layer hyperparameters without degrading the algorithm’s performance – the modified network produces 0% training error (out of 50,000 examples) and  $\lesssim 2.5\%$  test error (out of 10,000 examples) on MNIST using a network with three hidden layers and no regularization term in its cost function. These error rates are comparable to those of other biologically-motivated networks [Bartunov et al., 2018] and are approximately the same as those of the layered network with unique, manually-tuned learning rates in [Scellier and Bengio, 2016]. Our method could be implemented with relative ease in any system with configurable connectivity, such as those already described in several neuromorphic hardware platforms [Davies et al., 2018; Schemmel et al., 2010; Shainline et al., 2019]. Layer-skipping connections have been observed in biological brains [Bullmore and Sporns, 2009], so the approach is biologically-plausible. Similar techniques have seen success in convolutional [He et al., 2015; Srivastava et al., 2015a] and multilayer feedforward [Xiaohu et al., 2011; Krishnan et al., 2019] networks. Our findings outlined in this paper suggest that layer-skipping connections are effective-enough to be appealing in contexts where simplicity and biological plausibility are important.

## 2 BACKGROUND

### 2.1 Equilibrium propagation

Similarly to backpropagation, the equilibrium propagation algorithm [Scellier and Bengio, 2016] trains networks by approximating gradient descent on a cost function. Equilibrium propagation is applicable to any network with dynamics characterized by evolution to a fixed point of an associated energy function; our implementation is a recreation of that in [Scellier and Bengio, 2016], which applies it to a continuous Hopfield network [Hopfield, 1984]. The mathematical formulation of the framework can be found in [Scellier and Bengio, 2016]. We discuss its appeal over backpropagation in section 5.1.

#### 2.1.1 Implementation in a continuous Hopfield network

Here we summarize the equations through which a continuous Hopfield network is trained using equilibrium propagation; this summary is based on the more-thorough and more-general treatment in [Scellier and Bengio, 2016].

Consider a network with  $n$  neurons organized into an input layer with  $p$  neurons, hidden layers with  $q$  neurons and an output layer with  $r$  neurons. Let the activations of these neurons be denoted respectively by vectors  $\mathbf{x} \in \mathbb{R}^p$ ,  $\mathbf{h} \in \mathbb{R}^q$  and  $\mathbf{y} \in \mathbb{R}^r$ , and let  $\mathbf{s} = (\mathbf{h}^T, \mathbf{y}^T)^T \in \mathbb{R}^{q+r}$  and  $\mathbf{u} = (\mathbf{x}^T, \mathbf{s}^T)^T \in \mathbb{R}^n$  be vectors of, respectively, the activations of non-fixed (non-input) neurons and of all neurons in the network. Let  $\mathbf{W} \in \mathbb{R}^{n \times n}$  and  $\mathbf{b} \in \mathbb{R}^n$  denote the network's weights and biases where  $w_{ij}$  is the connection weight between neurons  $i$  and  $j$  and  $b_i$  is the bias for neuron  $i$  ( $\forall i$   $w_{ii} = 0$  to prevent self-connections), and let  $\rho$  denote its activation function; here and in [Scellier and Bengio, 2016],

$$\rho(x) = \begin{cases} 0 & x < 0 \\ x & 0 \leq x \leq 1 \\ 1 & x > 1 \end{cases} \quad (1)$$

is a hardened sigmoid function where  $\rho'(0) = \rho'(1)$  is defined to be 1 to avoid neuron saturation. Let  $\boldsymbol{\rho}((x_1, \dots, x_n)^T) = (\rho(x_1), \dots, \rho(x_n))^T$ .

The behavior of the network is to perform gradient descent on a total energy function  $F$  that is modified by a training example  $(\mathbf{x}_d, \mathbf{y}_d)$ . Consider energy function  $E : \mathbb{R}^n \rightarrow \mathbb{R}$ ,

$$E(\mathbf{u}; \mathbf{W}, \mathbf{b}) = \frac{1}{2} \mathbf{u}^T \mathbf{u} - \frac{1}{2} \boldsymbol{\rho}(\mathbf{u})^T \mathbf{W} \boldsymbol{\rho}(\mathbf{u}) - \mathbf{b}^T \mathbf{u} \quad (2)$$

and arbitrary cost function  $C : \mathbb{R}^r \rightarrow \mathbb{R}_+$ ; here and in [Scellier and Bengio, 2016] it is a quadratic cost function given by

$$C(\mathbf{y}) = \frac{1}{2} \|\mathbf{y} - \mathbf{y}_d\|_2^2, \quad (3)$$

though the framework still works for cost functions incorporating a regularization term dependent on  $\mathbf{W}$  and  $\mathbf{b}$ . The total energy function  $F : \mathbb{R}^n \rightarrow \mathbb{R}$  is given by

$$F(\mathbf{u}; \beta, \mathbf{W}, \mathbf{b}) = E(\mathbf{u}; \mathbf{W}, \mathbf{b}) + \beta C(\mathbf{y}) \quad (4)$$

where the clamping factor  $\beta$  is a small constant.  $\mathbf{s}$  evolves over time  $t$  as

$$\frac{d\mathbf{s}}{dt} \propto -\frac{\partial F}{\partial \mathbf{s}}. \quad (5)$$

Equilibrium has been reached when  $\frac{\partial F}{\partial \mathbf{s}} \approx 0$ . This can be viewed as solving the optimization problem

$$\underset{\mathbf{s} \in \mathbb{R}^{q+r}}{\text{minimize}} F((\mathbf{x}_d^T, \mathbf{s}^T)^T; \beta, \mathbf{W}, \mathbf{b}) \quad (6)$$

by using gradient descent to find a local minimum of  $F$ .

The procedure for training on a single input-output pair  $(\mathbf{x}_d, \mathbf{y}_d)$  is as follows:

1. Clamp  $\mathbf{x}$  to  $\mathbf{x}_d$  and perform the free-phase evolution: evolve to equilibrium on the energy function  $F(\mathbf{u}; 0, \mathbf{W}, \mathbf{b})$  in a manner dictated by equation 5. Record the equilibrium state  $\mathbf{u}^0$ .
2. Perform the weakly-clamped evolution: evolve to equilibrium on the energy function  $F(\mathbf{u}; \beta, \mathbf{W}, \mathbf{b})$  using  $\mathbf{u}^0$  as a starting point. Record the equilibrium state  $\mathbf{u}^\beta$ .

90 3. Compute the correction to each weight in the network:

$$\Delta W_{ij} = \frac{1}{\beta}(\rho(u_i^\beta)\rho(u_j^\beta) - \rho(u_i^0)\rho(u_j^0)). \quad (7)$$

91 Adjust the weights using  $W_{ij} \leftarrow W_{ij} + \alpha\Delta W_{ij}$  where the learning rate  $\alpha$  is a positive constant.

92 4. Compute the correction to each bias in the network:

$$\Delta b_i = \frac{1}{\beta}(\rho(u_i^\beta) - \rho(u_i^0)) \quad (8)$$

93 and adjust the biases using  $b_i \leftarrow b_i + \alpha\Delta b_i$ .

94 This can be repeated on as many training examples as desired. Training can be done on batches by  
 95 computing  $\Delta W_{ij}$  and  $\Delta b_i$  for each input-output pair in the batch, and correcting using the averages of  
 96 these values. Note that the correction to a weight is computed using only the activations of neurons it  
 97 directly affects, and the correction to a bias is computed using only the activation of the neuron it directly  
 98 affects. This contrasts with backpropagation, where to correct a weight or bias  $l$  layers from the output it is  
 99 necessary to know the activations, derivatives and weights of all neurons between 0 and  $l - 1$  layers from  
 100 the output.

## 101 2.2 Vanishing gradient problem

102 Vanishing gradients are problematic because they reduce a network's rate of training and could be  
 103 difficult to represent in neuromorphic analog hardware due to limited bit depth. As a simple example, the  
 104 multiplicative factor of 0.008 used in previous implementations would lead to significant precision errors  
 105 in a system with signals represented by integers from 0-16 (bit depth of 4).

106 The vanishing gradient problem is familiar in the context of conventional feedforward networks, where  
 107 techniques such as the weight initialization scheme in [Glorot and Bengio, 2010], the use of activation  
 108 functions with derivatives that do not lead to output saturation [Schmidhuber, 2015], and batch norma-  
 109 lization [Ioffe and Szegedy, 2015] have been effective at overcoming it. However, in the context of the  
 110 networks trained in [Scellier and Bengio, 2016], the vanishing gradient problem persists even when the  
 111 former two techniques are used. To our knowledge batch normalization has not been used in the context of  
 112 equilibrium propagation; however, it seems unlikely to be biologically-plausible.

## 3 IMPLEMENTATION

We recreated the equilibrium propagation implementation<sup>1</sup> in [Scellier and Bengio, 2016] using the Pytorch library. Like the networks in [Scellier and Bengio, 2016], our networks are continuous Hopfield networks with a hardened sigmoid activation function

$$\sigma(x) = \text{Max}\{0, \text{Min}\{x, 1\}\}$$

and squared-error cost function with no regularization term

$$C = ||\mathbf{y} - \mathbf{y}_d||_2^2,$$

<sup>1</sup> [https://github.com/jgammell/Equilibrium\\_Propagation\\_mobile.git](https://github.com/jgammell/Equilibrium_Propagation_mobile.git)

where  $\mathbf{y}$  is the network's output and  $\mathbf{y}_d$  is the target output. Tests were run on MNIST [LeCun and Cortes, 1998] grouped into batches of 20 examples, with the 50,000 training examples used for training and the 10,000 validation examples used for computing test errors.

We use two performance-enhancing techniques that were used in [Scellier and Bengio, 2016]: we randomize the sign of  $\beta$  before training on each batch, which has a regularization effect, and we use persistent particles, where the state of the network after training on a given batch during epoch  $n$  is used as the initial state for that batch during epoch  $n + 1$ . Persistent particles reduce the computational resources needed to approximate the differential equation governing network evolution, and would be unnecessary in an analog implementation that can approximate the equation efficiently. Note that this technique leads to higher error rates early in training than would be present with a more-thorough approximation of the differential equation.

### 3.1 Layered topology with per-layer rates

We recreated the 5-layer network evaluated in [Scellier and Bengio, 2016]. It has the standard layered topology shown in figure 1, and consists of a 784-neuron input layer, 3 500-neuron hidden layers and a 10-neuron output layer. Weights are initialized using the scheme from [Glorot and Bengio, 2010]. As mentioned above, each layer has a unique learning rate; the rates are  $\alpha_1 = .128$ ,  $\alpha_2 = .032$ ,  $\alpha_3 = .008$  and  $\alpha_4 = .002$  where  $\alpha_i$  is the learning rate for the connection weights between layers  $i$  and  $i + 1$  and for the biases in layer  $i$ , and the input and output layers are denoted  $i = 1$  and  $i = 5$ , respectively.

### 3.2 Layered topology with global learning rate

To illustrate the vanishing gradient problem and provide a point of reference, we also tested the network in section 3.1 with a single global learning rate of .02.

### 3.3 Our topology

---

#### Algorithm 1: Algorithm to produce our topology

---

**Input:** Layered network from section 3.2

**Input:** Integer  $n$ , giving number of connections to replace

**Output:** A network with our modified topology

**for** hidden layer in network **do**

  Add edge between each pair of neurons in layer

**for**  $i \leftarrow 1$  **to**  $n$  **do**

  Randomly select pre-existing connection in network;

  Add connection between random unconnected pair of neurons in network;

  // Do not allow self connections

  // Do not allow connections between two input neurons or between two output neurons

  Remove pre-existing connection;

**return** modified network

---

To generate a network with our topology, we use algorithm 1. This topology is illustrated in figure 2. The above algorithm is approximately equivalent to the algorithm for generating a small-world network described in [Watts and Strogatz, 1998] with  $p = 1 - (\frac{N_o - 1}{N_o})^n$  for  $p \lesssim .2$ , where  $N_o$  is the number of connections in the network; to contextualize the number of replaced connections we will henceforth describe networks with our topology in terms of  $p$  instead of  $n$ . We have seen good results with  $p \approx 8\%$ . We have seen similar results when connections are added to the network, rather than randomly replaced (algorithm 1, without removing pre-existing connections).

For these networks we use a global learning rate of .02 and, as in the networks from sections 3.1 and 3.2, initialize connections between neurons in adjacent layers using the scheme from [Glorot and Bengio, 2010]. For all other connections we draw initial weights from the uniform distribution  $U[-.05, .05]$  where the value .05 was determined empirically to yield good results.

## 4 RESULTS

We compared the networks described in section 3 by observing their behavior while training on MNIST [LeCun and Cortes, 1998]. All networks used  $\epsilon = .5$ ,  $\beta = 1.0$ , 500 free-phase iterations, 8 weakly-clamped-phase iterations, and were trained for 250 epochs.

### 4.1 Network performance comparison

Figure 3 illustrates that our network significantly outperforms one with a global learning rate, and achieves close to the same training and test error rates as one with unique learning rates, albeit after around 25% more epochs. Both our network and the layered network with unique learning rates achieve approximately a 2.5% test error and 0% training error, whereas the layered network with a global learning rate has test and training error rates around .5% higher than the other two networks.

### 4.2 Training rates of individual pairs of layers

To observe the extent of the vanishing gradient problem, for each network we tracked the root-mean-square correction to weights in each of its layers during training on MNIST [LeCun and Cortes, 1998]. Figure 4 shows an 11-point centered moving average of these values (without averaging the values are very volatile). It can be seen that for the layered network with a global learning rate, the magnitude of the correction to a typical neuron vanishes with depth relative to the output, with the shallowest weights training around 100 times faster than the deepest weights - this illustrates the vanishing gradient problem. The use of unique learning rates is very effective at making corrections uniform. Our topology with  $p = 7.56\%$  is effective at making deeper layers train in a uniform way, but the output layer still trains around 10 times faster than deeper layers; nonetheless, figure 3 suggests that this imperfect solution still yields a significant performance benefit.

The fast training of the output layer in the network with our topology is probably because no layer-skipping connections attach directly to the target output, so for any value of  $p$  the shortest path between a deep neuron and the target layer is at least 2 connections long, whereas the path between an output neuron and the target layer is only 1 connection long.

### 4.3 Effect of $p$

We tracked the training error after one epoch of a network with our topology while varying  $p$ ; the results are shown in figure 5. For  $p < .1\%$ , there is little improvement in the error rate as  $p$  is increased, but there is substantial improvement in the uniformity of the training rates of deep layers. When  $p > .1\%$ , the deep layers are very uniform, and the error rate starts decreasing with  $p$  at a rate that is slightly slower than exponential; at this point there is little improvement in the uniformity of deep layers, but the rate of the shallowest layer appears to move closer to those of the deeper layers.

We found that our topology performs significantly worse than the basic topology with one learning rate when few connections are replaced. This could be due to a poor weight initialization scheme for the added intralayer connections; we have noticed anecdotally that networks appear to be less-sensitive to their weight initialization scheme as connections are replaced. We have found that networks perform poorly relative to a basic network with one learning rate until  $p$  is in the ballpark of 7%. This experiment suggests that training rate will keep improving long after that, but does not show long-term performance or test performance; we suspect that a network’s generalization ability will suffer for large  $p$  as it loses its regimented nature.

## 5 DISCUSSION

### 5.1 Comparing the computational complexity of equilibrium propagation and backpropagation

The main motivations for using equilibrium propagation instead of an alternative machine learning technique (such as deep learning using backpropagation for training) are 1) to gain insight into the operation of the brain by developing target-based learning approaches in biologically plausible networks and 2) to develop algorithms that are more easily implemented in hardware. Below we qualitatively compare the hardware that would be needed for implementation of equilibrium propagation versus for backpropagation on a standard feedforward network to gain insight into the utility of these networks.

#### 5.1.1 Requirements of equilibrium propagation

Just as in the algorithm, to implement equilibrium propagation in hardware, three different phases of hardware operation are required. In the first (free) phase, it follows from equations 2, 4 and 5 that to determine its state, the  $i$ -th neuron in a network must compute

$$\frac{\partial F}{\partial u_i} = u_i - \frac{1}{2} \rho'(u_i) \left[ \sum_{i \neq j} W_{ij} \rho(u_j) + b_i \right],$$

plus the term  $\beta(u_i - y_i^{target})$  for output neurons when using a squared-error cost function, and then integrate the result over time. Parameter correction rules are given by equations 7 and 8. This is exactly the operation of an analog leaky integrate and fire neuron, as for example implemented in the neuromorphic hardware platforms of references [Indiveri et al., 2011; Schemmel et al., 2010] among others. A qualitative diagram of potential neuron and synapse devices and their output and read/write to memory operations are shown in the diagram in figure 6 (a). At each neuron  $N_i^l$  the value of  $U_{i,0}^{l+1}$  is written to memory and the nonlinear function  $\rho$  is applied before sending to the synapse device, where it is multiplied by the weight  $w_{ij}^{l+1}$  which is read from memory by the synapse device. These weighted outputs are summed at the input of the next neuron device ( $N_j^{l+1}$ ) and added to a bias value  $b_j^{l+1}$  that is read from memory to generate  $U_{l+1}$ .

In the second (weakly-clamped) phase, shown in figure 6 (b), the operation of the hardware is exactly the same as in (a), with the value  $U_\beta$  written to memory at each neuron. Not shown in figure 6 is the functionality at the output neurons which are weakly clamped and have a new function in this phase.

Finally, in the third phase, the weights and biases are updated as shown in figure 6 (c). At each neuron device the values of  $U_0$  and  $U_\beta$  are read from memory and  $\rho(U_0)$  and  $\rho(U_\beta)$  are calculated. At the synapse device, the computation of equation 7 is performed using these values from the pre- and post-synaptic neurons to calculate the weight update  $\Delta w$ , and the value of the weight in memory is updated to  $w + \alpha \Delta w$ . Similar updates are applied to the bias  $b$  at every neuron according to equation 8. As shown at the top of 6, for  $N$  such neurons per layer, there will be  $N^2$  synapses.

#### 5.1.2 Requirements of backpropagation

Backpropagation is an algorithm for training networks using gradient descent. It is most typically applied to feedforward neural networks, in which the activation value of a neuron  $i$  in layer  $l$  is given by

$$\rho(u_i^l) = \rho\left(\sum_j W_{ij}^l u_j^{l-1} + b_i^l\right).$$

This is very similar to the free running situation in equilibrium propagation, with the main difference being that the connections are unidirectional. The qualitative implementation of this inference phase in



hardware is shown in Fig. 7 (a). Using backpropagation, the parameters are then updated by computing error correction terms  $\delta_i^l$  for each neuron  $i$  in layer  $l$ ; for the output layer  $L$  the correction is

$$\delta_i^L = \rho'(u_i^L)(\rho(u_i^L) - y_i^{target})$$

and for deeper layers it is

$$\delta_i^l = \rho'(u_i^l) \sum_j W_{ij}^{l+1} \delta_j^{l+1}.$$

The implementation of this in hardware is shown in figure 7 (b) (excluding layer  $L$ ). Note that the data is now moving in the opposite (backwards) direction, and unlike in the case of equilibrium propagation, the functions implemented by the neurons are entirely different to the operation in the forward phase shown in (a). In a final phase, weights are corrected using

$$\Delta W_{ij}^l = \rho(u_i^{l-1}) \delta_j^l$$

and biases using

$$\Delta b_i^l = \delta_i^l.$$

212 This is shown in figure 7 (c).

### 213 5.1.3 Comparison

214 The most-significant difference between the algorithms is that in equilibrium propagation, the free  
215 and weakly-clamped phases of training are identical for most neurons and the weakly-clamped phase  
216 requires only slight modification to output neurons, whereas in backpropagation these phases demand  
217 significantly-different functionality from essentially all neurons. There are two other differences that we do  
218 not believe to be significant in terms of ease of implementation in hardware. One is that in equilibrium  
219 propagation each pair of neurons is joined by a bidirectional synapse, whereas in backpropagation each pair  
220 is joined by two unidirectional synapses; we expect both cases to be equally easy to implement. The other is  
221 that in equilibrium propagation, each neuron must remember its equilibrium state after the free phase while  
222 it executes the weakly-clamped phase; since backpropagation implies a state variable for the activation and  
223 error term of each neuron, the memory requirement of each neuron should be the same in both cases. For  
224 a hardware implementation, the need for distinct free and weakly-clamped phases (temporally non-local  
225 credit assignment) significantly reduces the advantages associated with the spatially local credit assignment.  
226 Recently there has been new work that indicates that the algorithm can be modified to eliminate the need  
227 for both phases [Ernault et al., 2020]. This would significantly reduce the memory requirements of the  
228 algorithm. Various characteristics of both algorithms are compared side-by-side in table 1.

## 229 5.2 Related work

230 References [Lee et al., 2015; Xie and Seung, 2003; Pineda, 1987] describe other approaches to locally  
231 approximating the gradient of a cost function. References [Lillicrap et al., 2014; Crafton et al., 2019]  
232 explore the use of a random feedback matrix for backwards connections that is more biologically-plausible  
233 than identical forwards and backwards connections. Reference [Bartunov et al., 2018] explores the present  
234 state of biologically-motivated deep learning, and [Bengio et al., 2015] discusses the criteria a biologically-  
235 plausible network would need to satisfy. References [Shainline et al., 2019; Davies et al., 2018; Nahmias  
236 et al., 2013] discuss analog hardware that could potentially implement equilibrium propagation. References  
237 [He et al., 2015; Srivastava et al., 2015a; Xiaohu et al., 2011; Krishnan et al., 2019] use layer-skipping  
238 connections for other types of networks and learning frameworks. References [Ioffe and Szegedy, 2015;  
239 Glorot and Bengio, 2010] give approaches to solving vanishing gradient problems.



### 240 5.3 Directions for Future Research

241 There are several directions in which future research could be taken:

- 242 • Evaluating the effectiveness of this approach on hard datasets, such as CIFAR and ImageNet.
- 243 • Evaluating the effect of  $p$  on a network's test error in the long term.
- 244 • Exploring the effectiveness of layer-skipping connections on deeper networks.
- 245 • Exploring the effectiveness of a network when layer-skipping connections are used during training and
- 246 removed afterwards.

### CONFLICT OF INTEREST STATEMENT

247 The authors declare that the research was conducted in the absence of any commercial or financial  
248 relationships that could be construed as a potential conflict of interest.

249 The U.S. Government is authorized to reproduce and distribute reprints for governmental purposes  
250 notwithstanding any copyright annotation thereon.

### REFERENCES

- 251 Bartunov, S., Santoro, A., Richards, B. A., Hinton, G. E., and Lillicrap, T. P. (2018). Assessing the  
252 scalability of biologically-motivated deep learning algorithms and architectures. *CoRR* abs/1807.04587
- 253 Bengio, Y., Lee, D., Bornschein, J., and Lin, Z. (2015). Towards biologically plausible deep learning.  
254 *CoRR* abs/1502.04156
- 255 Bullmore, E. and Sporns, O. (2009). Complex brain networks: graph theoretical analysis of structural and  
256 functional systems. *Nature*
- 257 Crafton, B., Parihar, A., Gebhardt, E., and Raychowdhury, A. (2019). Direct feedback alignment with  
258 sparse connections for local learning. *CoRR* abs/1903.02083
- 259 Davies, M., Srinivasa, N., Lin, T.-H., Chinya, G., Joshi, P., Lines, A., et al. (2018). Loihi: A neuromorphic  
260 manycore processor with on-chip learning. *IEEE Micro* PP, 1–1. doi:10.1109/MM.2018.112130359
- 261 Ernoult, M., Grollier, J., Querlioz, D., Bengio, Y., and Scellier, B. (2020). Equilibrium propagation with  
262 continual weight updates
- 263 Glorot, X. and Bengio, Y. (2010). Understanding the difficulty of training deep feedforward neural  
264 networks. In *Proceedings of the Thirteenth International Conference on Artificial Intelligence and*  
265 *Statistics*, eds. Y. W. Teh and M. Titterton (Chia Laguna Resort, Sardinia, Italy: PMLR), vol. 9 of  
266 *Proceedings of Machine Learning Research*, 249–256
- 267 He, K., Zhang, X., Ren, S., and Sun, J. (2015). Deep residual learning for image recognition. *CoRR*  
268 abs/1512.03385
- 269 Hopfield, J. (1984). Neurons with graded response have collective computational properties like those of  
270 two-state neurons. *Proceedings of the National Academy of Sciences of the United States of America* 81,  
271 3088–92. doi:10.1073/pnas.81.10.3088
- 272 Indiveri, G., Linares-Barranco, B., Hamilton, T., van Schaik, A., Etienne-Cummings, R., Delbruck, T., et al.  
273 (2011). Neuromorphic silicon neuron circuits. *Frontiers in Neuroscience* 5, 73. doi:10.3389/fnins.2011.  
274 00073
- 275 Ioffe, S. and Szegedy, C. (2015). Batch normalization: Accelerating deep network training by reducing  
276 internal covariate shift. *CoRR* abs/1502.03167
- 277 Krishnan, G., Du, X., and Cao, Y. (2019). Structural pruning in deep neural networks: A small-world  
278 approach
- 279 [Dataset] LeCun, Y. and Cortes, C. (1998). The mnist database of handwritten digits

- 280 Lee, D.-H., Zhang, S., Fischer, A., and Bengio, Y. (2015). Difference target propagation. 498–515.  
 281 doi:10.1007/978-3-319-23528-8\_31
- 282 Lillicrap, T. P., Cownden, D., Tweed, D. B., and Akerman, C. J. (2014). Random feedback weights support  
 283 learning in deep neural networks
- 284 Nahmias, M., Shastri, B., Tait, A., and Prucnal, P. (2013). A leaky integrate-and-fire laser neuron for  
 285 ultrafast cognitive computing. *Selected Topics in Quantum Electronics, IEEE Journal of* 19, 1–12.  
 286 doi:10.1109/JSTQE.2013.2257700
- 287 Pineda, F. (1987). Generalization of back-propagation to recurrent neural networks. *Physical Review*  
 288 *Letters* 59, 2229–2232
- 289 Scellier, B. and Bengio, Y. (2016). Equilibrium propagation: Bridging the gap between energy-based  
 290 models and backpropagation
- 291 Schemmel, J., Brüderle, D., Grübl, A., Hock, M., Meier, K., and Millner, S. (2010). A wafer-scale  
 292 neuromorphic hardware system for large-scale neural modeling. *Proceedings of 2010 IEEE International*  
 293 *Symposium on Circuits and Systems*, 1947–1950
- 294 Schmidhuber, J. (2015). Deep learning in neural networks: An overview. *Neural Networks* 61, 85–117.  
 295 doi:10.1016/j.neunet.2014.09.003
- 296 Shainline, J. M., Buckley, S. M., McCaughan, A. N., Chiles, J. T., Jafari Salim, A., Castellanos-Beltran,  
 297 M., et al. (2019). Superconducting optoelectronic loop neurons. *Journal of Applied Physics* 126, 044902.  
 298 doi:10.1063/1.5096403
- 299 Simonyan, K. and Zisserman, A. (2014). Very deep convolutional networks for large-scale image  
 300 recognition
- 301 Srivastava, R. K., Greff, K., and Schmidhuber, J. (2015a). Highway networks. *CoRR* abs/1505.00387
- 302 Srivastava, R. K., Greff, K., and Schmidhuber, J. (2015b). Training very deep networks
- 303 Watts, D. and Strogatz, S. (1998). Collective dynamics of 'small-world' networks. *Nature*
- 304 Wozniak, S., Pantazi, A., and Eleftheriou, E. (2018). Deep networks incorporating spiking neural dynamics.  
 305 *CoRR* abs/1812.07040
- 306 Xiaohu, L., Xiaoling, L., Jinhua, Z., Yulin, Z., and Maolin, L. (2011). A new multilayer feedforward small-  
 307 world neural network with its performances on function approximation. In *2011 IEEE International*  
 308 *Conference on Computer Science and Automation Engineering*
- 309 Xie, X. and Seung, H. (2003). Equivalence of backpropagation and contrastive hebbian learning in a  
 310 layered network. *Neural computation* 15, 441–54. doi:10.1162/089976603762552988

## FIGURES

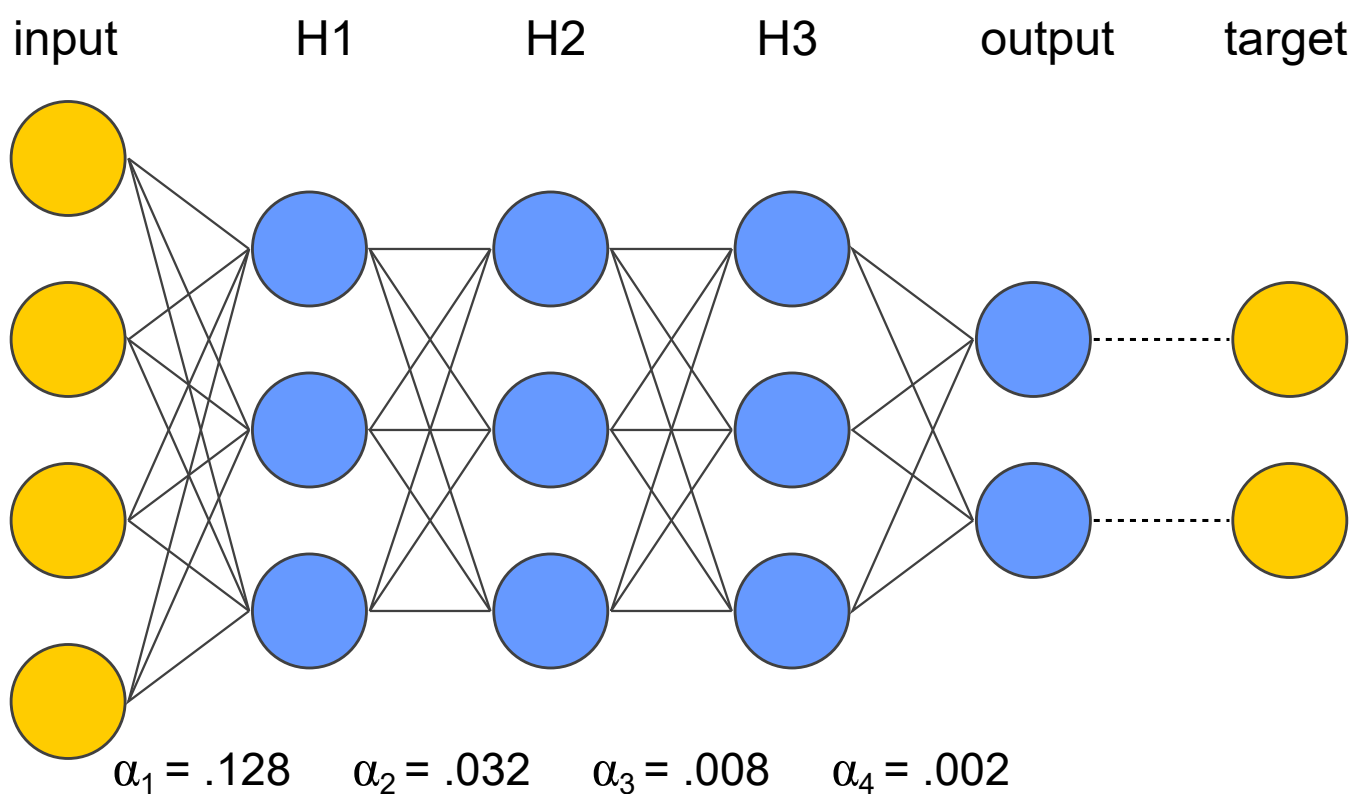


**Figure 1.** Topology of the layered network tested in [Scellier and Bengio, 2016]. All pairs of neurons in adjacent layers are connected. All connections are bidirectional. To compensate for the vanishing gradient problem, the learning rate  $\alpha$  is reduced by a factor of 4 each time distance from the output decreases by one layer.

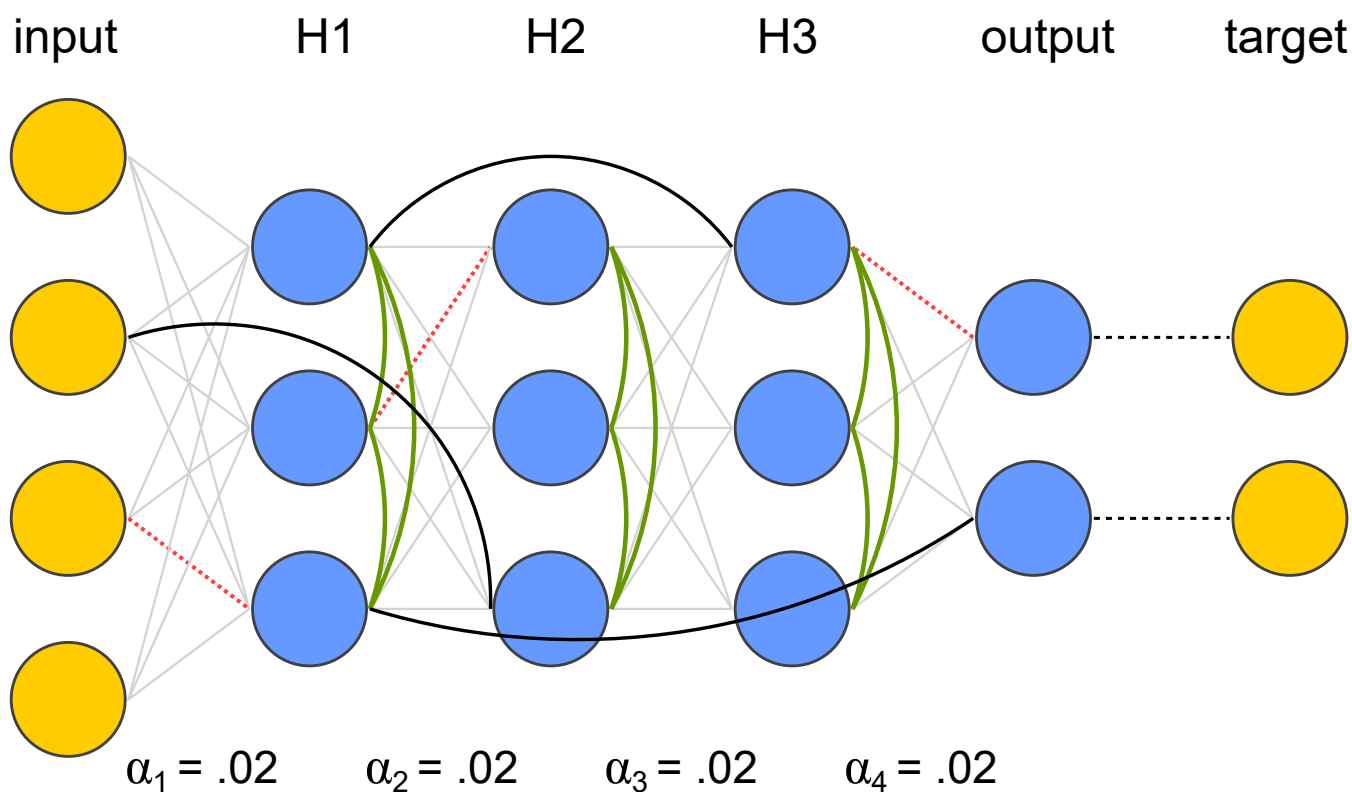


**Figure 2.** Our modifications to the topology of figure 1 to avoid a vanishing gradient while using a global learning rate. Red dotted lines denote connections that have been removed, black lines denote their replacements, and green solid lines denote added intralayer connections. All connections are bidirectional.

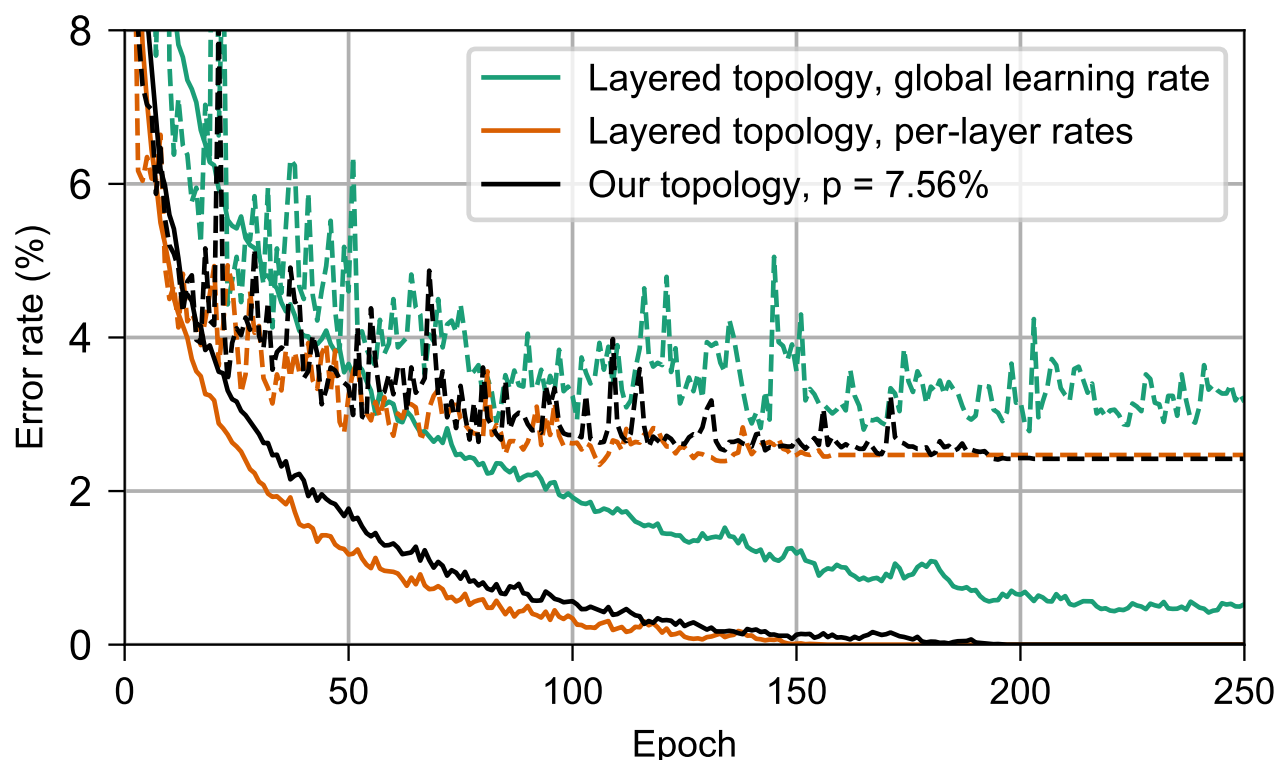


**Figure 3.** Performance on MNIST of the networks in section 3. Dashed lines show the test error and solid lines show the training error. In green is a layered network with a global learning rate (section 3.2), in orange is a layered network with per-layer rates individually tuned to counter the vanishing gradient problem (section 3.1), and in green is a network with our topology,  $p = 7.56\%$  (section 3.3). Observe that our topology is almost as effective as per-layer rates at countering the vanishing gradient problem that impedes training of the layered network with a global learning rate.

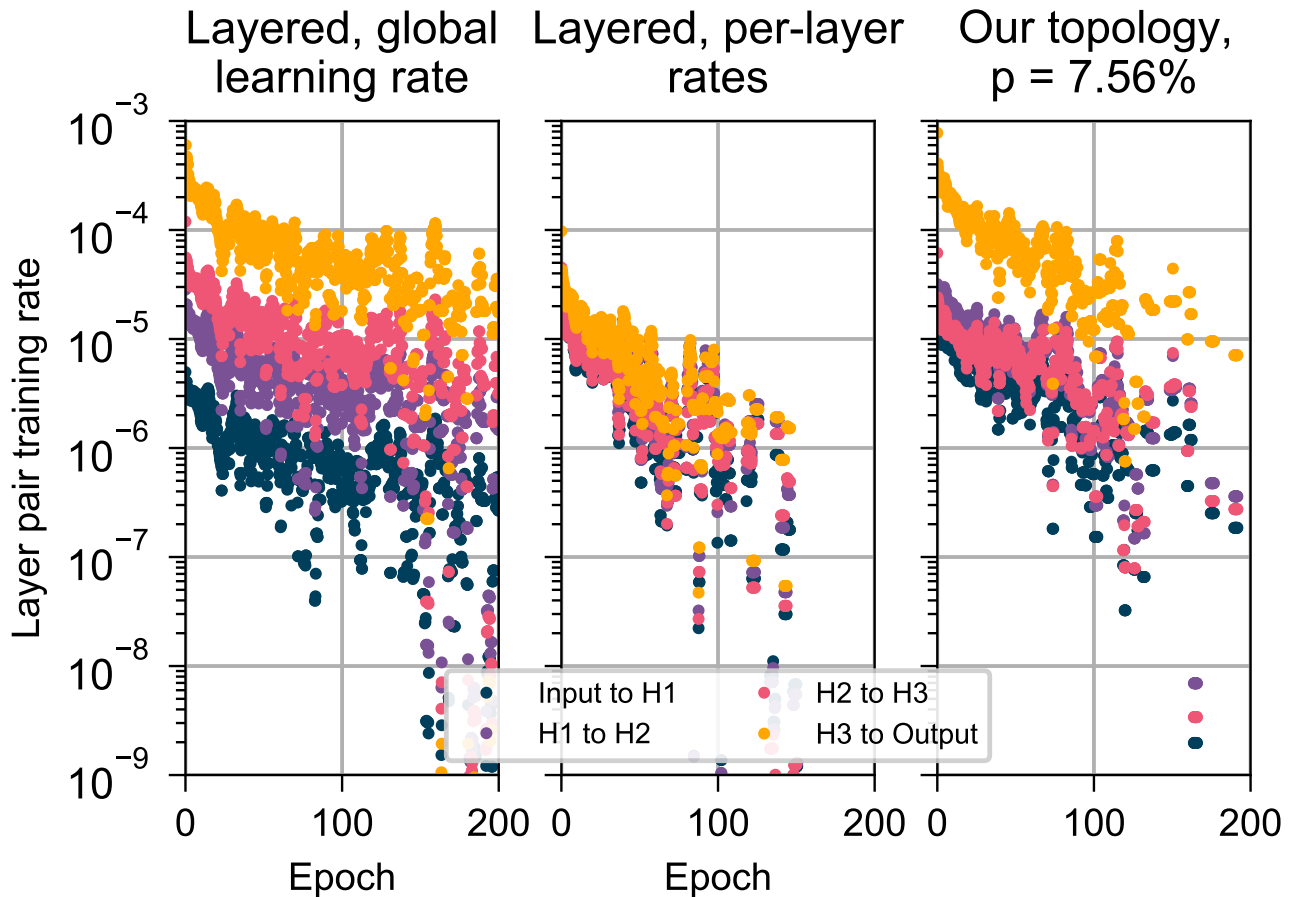


**Figure 4.** Root-mean-square corrections to weights in different layers while training on MNIST, for the networks in section 3. For clarity, values were subjected to an 11-point centered moving average. (left) A layered network with a single global learning rate (section 3.2). (center) A layered network a unique, individually-tuned learning rate for each layer (section 3.1). (right) A network with our topology,  $p = 7.56\%$  (section 3.3). Observe that the layered topology with a global learning rate has a vanishing gradient problem, which is almost completely solved by tuning an individual learning rate for each layer. Our topology improves the situation by making training uniform among the deeper layers, although the shallowest layer still trains more-quickly than the deeper layers.



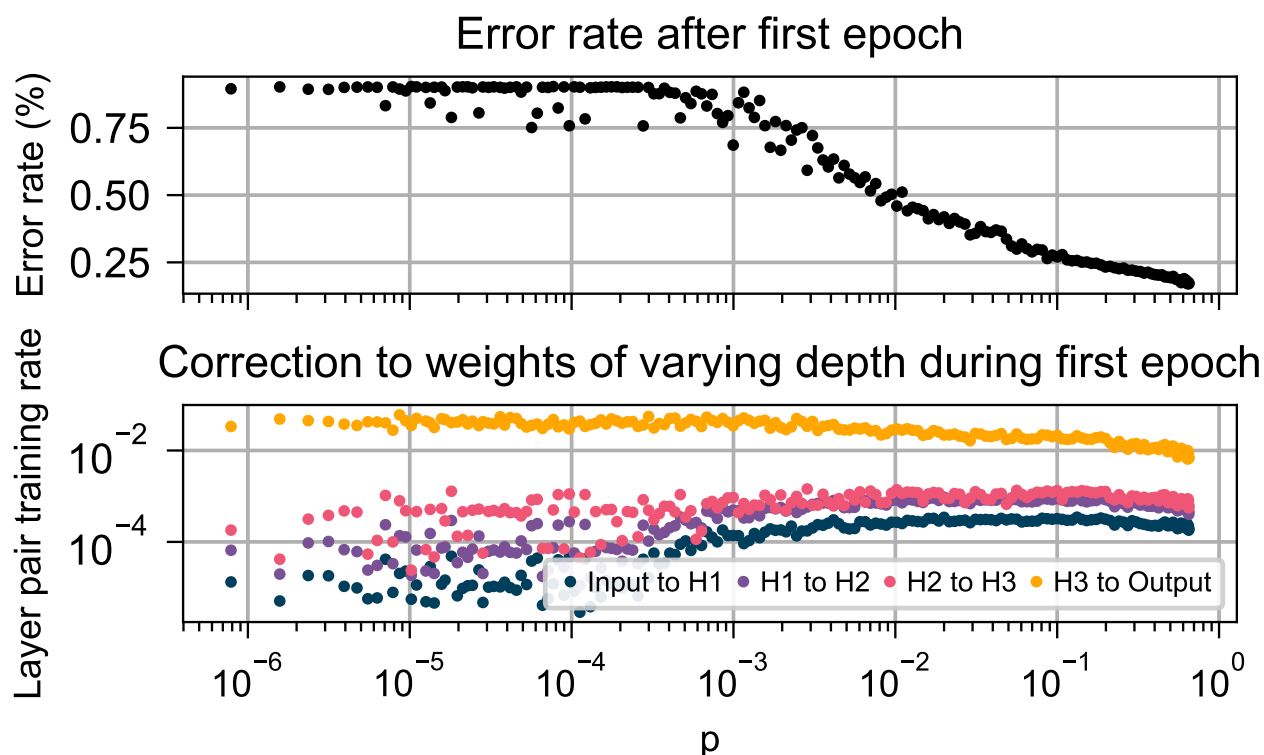


**Figure 5.** Behavior of our network (section 3.3) with varying  $p$ , during the first epoch of training. (top) The training error after one epoch. (bottom) Root-mean-square correction to weights in different layers during the first epoch. Observe that as  $p$  is increased, the error rate decreases and the root-mean-square corrections to each layer become more-uniform.

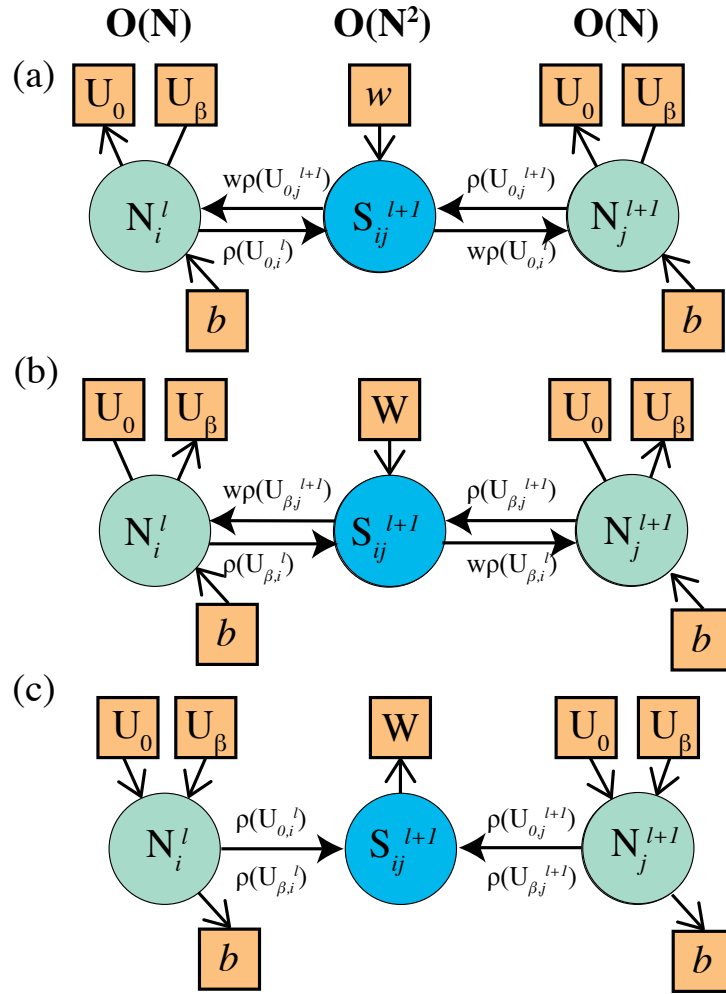


**Figure 6.** Illustration of the functionality needed to implement equilibrium propagation in hardware. Yellow squares indicate a value that must be stored in memory for a subsequent phase. The circles indicate ( $N$ ) neuron and ( $S$ ) synapse devices with the associated functions described in the text. (a) The functionality required by the neurons and synapses in the free running phase. (b) The functionality of the neurons and synapses (except output neurons) in the weakly clamped phase. (c) The functionality of the neurons and synapses in the weight and bias update phase.

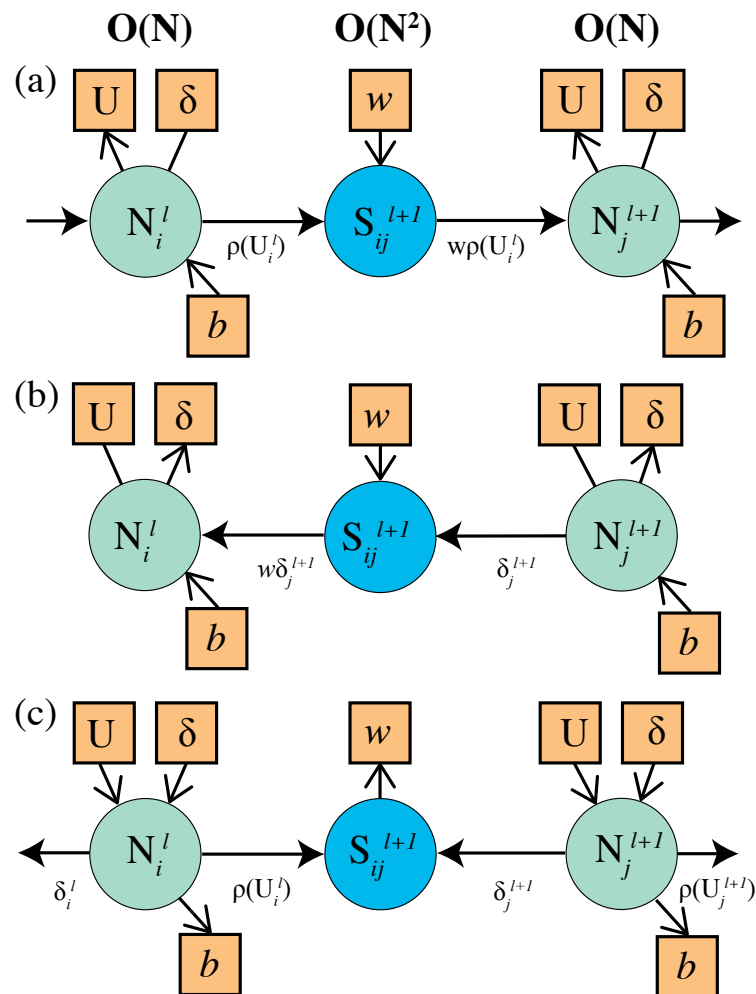


**Figure 7.** Illustration of the functionality needed to implement backpropagation in hardware. Yellow squares indicate a value that must be stored in memory for a subsequent phase. The circles indicate ( $N$ ) neuron and ( $S$ ) synapse devices with the associated functions described in the text. (a) The functionality required by the neurons and synapses in the forward pass phase. (b) The functionality of the neurons and synapses (except the last layer of neurons) in the backpropagation phase. (c) The functionality of the neurons and synapses in the weight and bias update phase.

## TABLES

	Backpropagation	Equilibrium Propagation
Number of distinct computations	2 – computations during forwards and backwards phases are distinct	$\approx 1$ – hidden neurons perform same computation in both phases. Output neurons perform a similar but modified version of the same computation.
Types of connections	Unidirectional to transmit activation to shallower neighbors and error to deeper neighbors	Bidirectional to each neighbor
Memory	Space to store activation and error term for each neuron	Space to store free and weakly-clamped activations for each neuron
Order of computations	Forwards propagation phase where layers are computed from deepest to shallowest; backwards propagation phase where layers are computed from shallowest to deepest; parameter update phase	Free phase where all neurons evolve simultaneously; weakly-clamped phase where all neurons evolve simultaneously; parameter update phase
Nonlinear activation function	Yes	Yes
Derivative of nonlinear activation function	Yes	Yes
Correction computation	Corrections require dedicated circuitry unique from that implementing propagation	Corrections require dedicated circuitry unique from that implementing evolution

**Table 1.** Comparison of the capabilities a hardware neuron would need in order to implement backpropagation and equilibrium propagation.